magnetochemistry

MDPI

Article

Rapid and Efficient Removal of Perchlorate from Environmental Water Samples by Magnetic Nanocomposite (Fe_3O_4@GO@MIL-53(Al)-NH_2)

Cong Hu [1,2], Limin Yan [1], Zuhai Bai [1], Mingzhong Xu [1], Yun Du [1,*] and Qiong Wang [1,*]

[1] Changsha Center for Diseases Prevention and Control, Changsha 410004, China; fox-winds@163.com (C.H.); looker200411@163.com (L.Y.); baizuhaicscdc@163.com (Z.B.); mzxuteam@126.com (M.X.)
[2] Hunan Provincial University Key Laboratory of Environmental Health and Risk Prevention and Control, Hengyang 421009, China
* Correspondence: hello_dudu1990@163.com (Y.D.); wangqiong4219@126.com (Q.W.); Tel.: +86-0731-85789979 (Y.D.); +86-0731-84717509 (Q.W.)

Abstract

Removing perchlorate from environmental water can effectively ensure the safety of drinking water and alleviate industrial and agricultural non-point source pollution. Nevertheless, the lack of adsorption sites in the existing adsorbents leads to low adsorption efficiency and low selectivity, which seriously hinders their further application. Here, we report a novel magnetic nanocomposite (Fe_3O_4@GO@MIL-53(Al)-NH_2) constructed on the basis of graphene oxide (GO) and metal-organic frameworks (MOFs, MIL-53(Al)-NH_2), as an efficient adsorbent for the removal of perchlorate from real environmental water samples. The Fe_3O_4@GO@MIL-53(Al)-NH_2 achieves efficient and selective adsorption of perchlorate through structure of the GO/MOFs composite. The Fe_3O_4@GO@MIL-53(Al)-NH_2 can be reused for four cycles. Its core advantages lie in: high capacity (23.31 mg g^{-1}), fast kinetics (2-min equilibrium), strong selectivity (anti-interference from co-existing anion ions), easy recovery (saturation magnetization value was 7.0 emu g^{-1}) and high perchlorate removal efficiency (RE%) of 90.2 ± 5.1%, providing an ideal adsorbent for the removal of perchlorate in contaminated water bodies.

Keywords: magnetic nanocomposite; Fe_3O_4@GO@MIL-53(Al)-NH_2; perchlorate; removal; environmental water samples

Check for updates

Academic Editors: Chu Dai and Chen Tian

Received: 14 September 2026
Revised: 21 October 2026
Accepted: 23 October 2026
Published: 26 October 2026

Copyright: © 2026 by the authors. Licensee MDPI, Basel, Switzerland. This article is an open access article distributed under the terms and conditions of the Creative Commons Attribution (CC BY) license.

1. Introduction

Perchlorate (ClO_4^-) is an inorganic anion with both natural and anthropogenic origins, among which anthropogenic activities constitute the dominant source. It is mainly released from military, aerospace, industrial production, fireworks manufacturing, and other fields [1–3]. As an emerging pollutant, perchlorate exhibits high water solubility, chemical stability, and poor degradability. Due to its excellent aqueous solubility, perchlorate readily migrates into surface and ground water, ultimately leading to aquatic environmental contamination [4,5]. Perchlorate predominantly accumulates in the human body through ingestion of drinking water and food, which poses substantial risks to human health. Existing literature has demonstrated that low-level perchlorate exposure disrupts normal human thyroid function by suppressing iodide uptake in thyroid tissue. This inhibitory effect curtails the biosynthesis of triiodothyronine (T_3) and thyroxine (T_4), thereby imposing health hazards on pregnant women, fetuses, and developing children [6,7]. Given

the adverse health effects induced by perchlorate exposure, the United States Environmental Protection Agency (USEPA) set a temporary health advisory reference concentration of 15 μg L^{-1} for perchlorate in 2009. Subsequently, the agency finalized a regulatory determination to mitigate perchlorate-related toxic risks under the Safe Drinking Water Act in 2011 [8]. A limit of 70 μg L^{-1} for perchlorate in drinking water was implemented in China in 2023 [9]. Hence, developing rapid and high-efficiency technologies for perchlorate removal from environmental water is of great practical significance for safeguarding public health.

Due to the high chemical stability and good aqueous solubility, perchlorate is difficult to remove from environmental water. Currently, the existing methods for perchlorate removal from environmental water mainly rely on chemical and physical removal techniques [2]. Common chemical removal methods include catalytic degradation [10], photocatalytic degradation [11], and electrochemical degradation [12]. However, chemical removal methods commonly exhibit drawbacks, including intricate operation and low removal efficiency, and the addition of catalysts in the reaction process may lead to secondary pollution. Compared with chemical removal, physical removal methods possess numerous advantages, such as simpler operational procedures and higher removal efficiency. The main physical removal methods for perchlorate include adsorption [13–18], ion exchange [19,20] and membrane filtration [21]. Activated carbon was the first adsorbent material applied to perchlorate removal. On this basis, carbon nanotubes, chitosans and other materials have also been employed to remove perchlorate from water samples. These adsorbents are cost-effective, but they rely solely on their pore structure for physical adsorption, which leads to sluggish adsorption kinetics and low removal efficiency. Furthermore, inferior regeneration performance restricts their cyclic reusability.

In recent years, Metal-organic frameworks (MOFs) have garnered extensive attention owing to their distinctive structures and promising application structure [22,23]. Owing to their unique topological architectures, large specific surface area and molecular sieving effect, MOFs serve as superior adsorbents [24]. To date, MOF-based adsorbents have been widely utilized for the removal of organic [25–29] and inorganic [30] pollutants in aqueous environments. Based on metal ions and organic ligands, MOFs can be classified into several series, such as MIL, ZIF, IRMOF, etc. Graphene oxide (GO) is a hydrophilic carbon-based adsorbent synthesized by chemical oxidation of graphene. As a single-layer carbon-based material, GO is functionalized with abundant polar groups (hydroxyl, carboxyl, and epoxy groups) on the surface. GO exhibits distinctive merits, including two-dimensional planar structure, excellent mechanical strength, good thermal and chemical stability, and large specific surface area [31,32].

In this work, a novel magnetic nanocomposite (Fe_3O_4@GO@MIL-53(Al)-NH_2) was prepared. Fe_3O_4@GO@MIL-53(Al)-NH_2 integrates the merits of GO and MOFs, including fast extraction kinetics, large specific surface area, high extraction efficiency and excellent selectivity. The as-prepared Fe_3O_4@GO@MIL-53(Al)-NH_2 was systematically characterized, and the experimental conditions were optimized. Under optimal conditions, the developed method was successfully applied for the removal of perchlorate from real environmental water samples.

2. Materials and Methods

2.1. Chemicals and Standards

Ferric chloride ($FeCl_3 \cdot 6H_2O$), ferrous chloride ($FeCl_2 \cdot 4H_2O$), aqueous ammonia ($NH_3 \cdot H_2O$), aluminum chloride ($AlCl_3 \cdot 6H_2O$), sodium chloride (NaCl), hydrochloric acid (HCl), sodium hydroxide (NaOH), N, N-dimethylformamide (DMF), sodium carbonate, and sodium bicarbonate were supplied by Sinopharm Chemical Reagent Co., Ltd. (Shang-

hai, China). 2-amino terephthalic acid was purchased from J&K Scientific Ltd. (Beijing, China). GO was purchased from XFNANO Co., Ltd. (Nanjing, China). All solid reagents and solvents used in this work were of analytical grade or higher. Perchlorate standard solution with a concentration of 1000 mg L^{-1} was supplied by NCS Testing Technology Co., Ltd. (Beijing, China). Ultrapure water with a resistivity of 18.2 MΩ·cm was produced using a PURELAB Chorus Ultrapure Water System (ELGA, High Wycombe, Buckinghamshire, UK).

2.2. Instruments

A Metrohm 930 ion chromatograph equipped with a suppressor and conductivity detector was employed for the qualitative and quantitative analysis of perchlorate. Chromatographic separation was performed on a Metrosep A Supp 4 anion column (4.0 mm × 250 mm, Metrohm, Herisau, Switzerland). The eluent consists of 4.0 mmol L^{-1} sodium carbonate and 1.7 mmol L^{-1} sodium bicarbonate. The flow rate was 1 mL min^{-1}, the column temperature was kept at 50 °C, and the injection volume was 200 μL.

IRAffinity-1S Fourier transform infrared spectroscopy (FT-IR) (SHIMADZU, Tkoyo, Japan) and Tecnai F30 transmission electron microscopy (TEM) (Hillsboro, OR, USA) were employed for characterization of the structure and morphology of the as-prepared nanocomposite, while ESCALAB250Xi X-ray photoelectron (XPS) (ThermoFisher Scientific, Waltham, MA, USA). D8 ADVANCE X-ray diffraction (XRD) (Bruker, Karlsruhe, Germany), LakeShore 7404 vibrating sample magnetometer (VSM) (LakeShore, Westerville, OH, USA), and Quantachrome NovaWin surface area analyzer (Quantachrome, Boynton Beach, FL, USA) were used for elemental composition and specific surface area measurements, respectively.

2.3. Preparation of Fe_3O_4@GO@MIL-53(Al)-NH_2

The synthetic procedure consisted of three stages as detailed below:

(1) Synthesis of Fe_3O_4 nanoparticles (NPs) [33]: In this work, the Fe_3O_4 NPs were synthesized via the co-precipitation method. Briefly, 0.05 mol $FeCl_3 \cdot 6H_2O$ and 0.025 mol $FeCl_2 \cdot 4H_2O$ were dissolved in 200 mL ultrapure water under a nitrogen atmosphere with continuous vigorous stirring at 85 °C. Subsequently, 20 mL of 30% $NH_3 \cdot H_2O$ was dropwise introduced into the above mixture, accompanied by elevated nitrogen flow and stirring speed; the orange-red solution instantly transformed into a black suspension. After a 6 h reaction period, the resulting suspension was cooled to ambient temperature naturally to yield Fe_3O_4 NPs. The as-prepared Fe_3O_4 NPs were repeatedly rinsed with ultrapure water until the filtrate reached neutral pH, followed by oven drying at 60 °C for 24 h.

(2) Synthesis of Fe_3O_4@GO: 1.5 g of pre-synthesized Fe_3O_4 NPs were dispersed in 100 mL of water solution under ultrasonication. Then 0.5 g of GO was added to the above suspension, and the mixture was stirred continuously for 6 h at 60 °C. The obtained precipitate was washed repeatedly with ultrapure water and dried under vacuum at 60 °C for 24 h.

(3) Synthesis of Fe_3O_4@GO@MIL-53(Al)-NH_2: The Fe_3O_4@GO@MIL-53(Al)-NH_2 nanocomposite was synthesized via a hydrothermal method. Briefly, 1.5 g $AlCl_3 \cdot 6H_2O$, 1 g pre-synthesized Fe_3O_4@GO and 0.8 g 2-amino terephthalic acid were dispersed in 30 mL ultrapure water, and the mixture was sealed in a Teflon-lined stainless steel autoclave and heated at 150 °C for 12 h. The precipitate was sequentially washed with ultrapure water and DMF, followed by drying to afford yellow Fe_3O_4@GO@MIL-53(Al)-NH_2.

2.4. Perchlorate Removal Experiments by Fe_3O_4@GO@MIL-53(Al)-NH_2

For removal experiments, a 1000 mg L^{-1} standard stock solution was purchased commercially. Briefly, 100 mg of Fe_3O_4@GO@MIL-53(Al)-NH_2 was dispersed into 200 mL environmental water sample (pH = 7) spiked with perchlorate at an initial concentration of 250 μg L^{-1}. Acetic acid and ammonia solution were used to adjust the pH of sample solutions. The suspension was stirred using a mechanical stirrer at 25 °C and 500 rpm for 2 min h to achieve rapid magnetic extraction of perchlorate. After extraction, the adsorbent was rapidly separated from the aqueous phase by an external magnetic field. The collected supernatant was filtered through a 0.22 μm microporous membrane prior to detection by ion chromatography. The removal efficiency (RE%) of perchlorate was calculated using the following equation:

$$RE\% = (C_o - C_t)*100\%/C_o \quad (1)$$

where C_o and C_t are the initial concentration and the residual concentration at time, respectively.

2.5. Recycle Experiments

To evaluate the recyclability and structural stability of the as-prepared Fe_3O_4@GO@MIL-53(Al)-NH_2, ten consecutive adsorption–desorption cycles were conducted with an initial perchlorate concentration of 250 μg L^{-1} and 100 mg Fe_3O_4@GO@MIL-53(Al)-NH_2. After each adsorption cycle, the Fe_3O_4@GO@MIL-53(Al)-NH_2 was immersed in 1 mol L^{-1} NaCl aqueous solution for 6 h to desorb loaded perchlorate anions, followed by rinsing with ultrapure water and overnight drying. The regenerated adsorbent was reused directly in the next cycle.

3. Results and Discussion

3.1. Characterization of Fe_3O_4@GO@MIL-53(Al)-NH_2

Transmission electron microscopy (TEM) was employed to characterize the morphology of Fe_3O_4@GO@MIL-53(Al)-NH_2. As shown in Figure 1a, Fe_3O_4@GO@MIL-53(Al)-NH_2 exhibits uniform granular morphology, with average particle sizes of ca. 20 nm.

The FT-IR spectra of Fe_3O_4, Fe_3O_4@GO and Fe_3O_4@GO@MIL-53(Al)-NH_2 are presented in Figure 1b. The characteristic absorption bond at 576 cm^{-1} was corresponds to stretching vibration of the Fe-O from Fe_3O_4. The absorption peaks at 1635 cm^{-1} correspond to the c=c stretching vibration of GO. The absorption peaks at 3382 cm^{-1} and 3496 cm^{-1} are the asymmetric and symmetric N-H stretching of the primary amine, respectively. Meanwhile, the peaks at 1388 cm^{-1} and 1574 cm^{-1} are attributed to the asymmetric/symmetric carboxylate stretches, respectively.

Vibrating sample magnetometry (VSM) characterization was added to evaluate the magnetization properties of Fe_3O_4@GO and Fe_3O_4@GO@MIL-53(Al)-NH_2. As shown in Figure 1c, the saturation magnetization value of Fe_3O_4@GO@MIL-53(Al)-NH_2 is measured to be 7.0 emu g^{-1}. This magnetic property enables rapid separation from aqueous solution during the adsorption process, significantly reducing operation time. Remarkably, Fe_3O_4@GO@MIL-53(Al)-NH_2 can be efficiently and rapidly isolated from an aqueous solution within 30 s through an applied magnetic field.

XRD was employed to characterize the crystalline structure of Fe_3O_4@GO, MIL-53(Al)-NH_2 and Fe_3O_4@GO@MIL-53(Al)-NH_2. As shown in Figure 1d, the diffraction patterns at 2θ of 31°, 35°, 43°, 54°, 57°, and 62° are observed, which are consistent with the standard reference card for Fe_3O_4 (ICDD PDF No. 00-19-0629). The diffraction patterns at 2θ of 10.5°, 15°, 17°, 18°, 20°, 25° and 28° are observed, which are consistent with the reference card for MIL-53(Al) (ICDD PDF No. 00-62-0907).

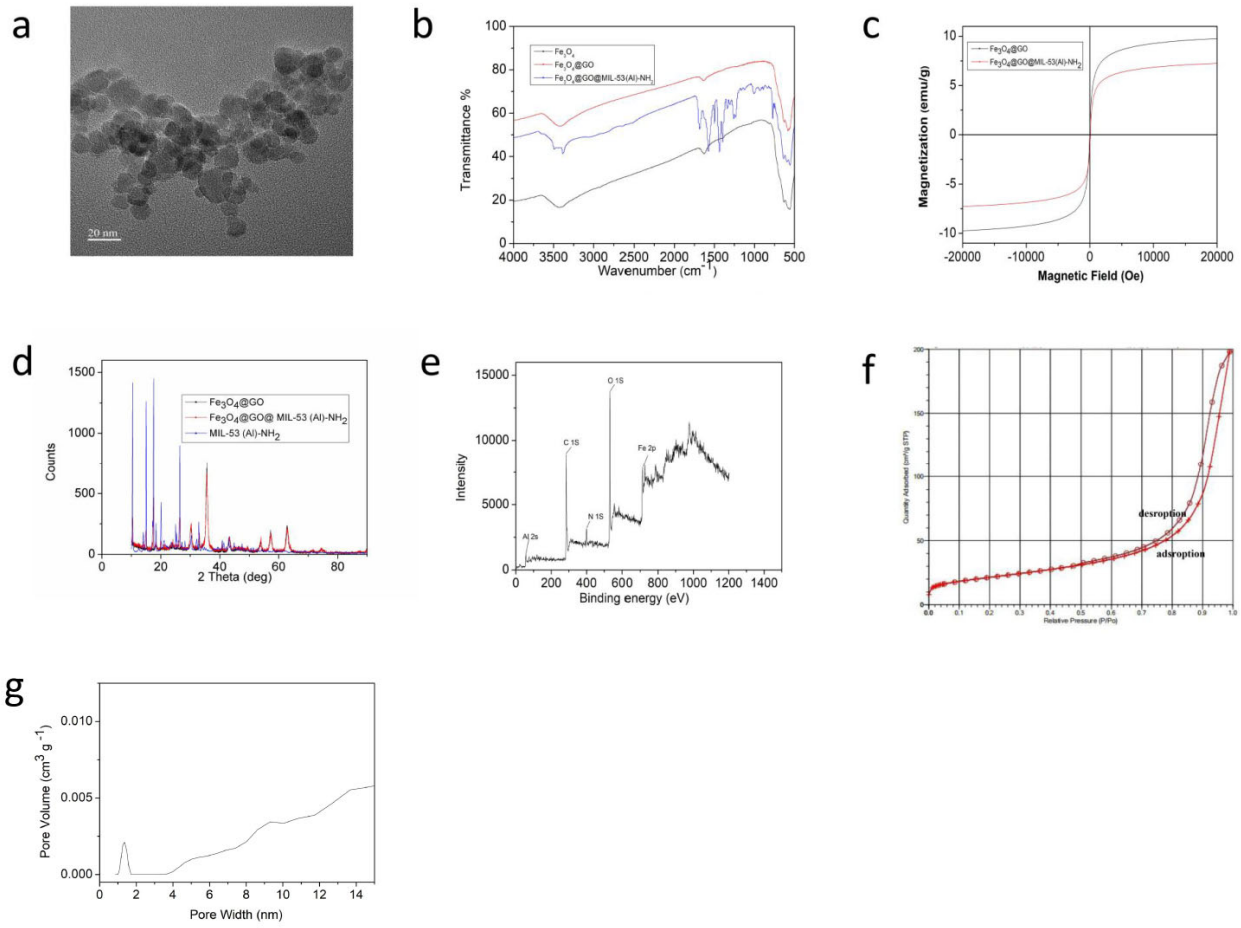


Figure 1. (**a**) TEM of Fe_3O_4@GO@MIL-53(Al)-NH_2; (**b**) FT-IR spectra of Fe_3O_4, Fe_3O_4@GO and Fe_3O_4@GO@MIL-53(Al)-NH_2; (**c**) VSM of Fe_3O_4@GO and Fe_3O_4@GO@MIL-53(Al)-NH_2; (**d**) XRD pattern of Fe_3O_4@GO, MIL-53(Al)-NH_2 and Fe_3O_4@GO@MIL-53(Al)-NH_2; (**e**) XPS spectra of Fe_3O_4@GO@MIL-53(Al)-NH_2; (**f**) N_2 adsorption–desorption isotherms; (**g**) pore size distribution curves of Fe_3O_4@GO@MIL-53(Al)-NH_2.

XPS was utilized to analyze the elemental composition of Fe_3O_4@GO@MIL-53(Al)-NH_2 and the XPS spectra are shown in Figure 1e. As summarized in Table 1, the Fe_3O_4@GO@MIL-53(Al)-NH_2 is composed of Al, N, Si, C, O, and Fe elements. Their corresponding atomic percentages (%) were 2.2, 3.5, 1.0, 59.0, 29.7, and 4.7, while the respective mass percentages (%) were 3.8, 3.1, 1.7, 44.8, 30.0, and 16.6. As shown in Table 1, the Si content in Fe_3O_4@GO is 0.1%, whereas it reaches 1% in Fe_3O_4@GO@MIL-53(Al)-NH_2. It can be speculated that Si was introduced during the synthesis process from Fe_3O_4@GO to Fe_3O_4@GO@MIL-53(Al)-NH_2, most likely originating from aluminum chloride or 2-amino terephthalic acid.

The surface porous structure of Fe_3O_4@GO@MIL-53(Al)-NH_2 was further investigated via BET. The N_2 adsorption–desorption isotherm curves and pore size distribution curves of Fe_3O_4@GO@MIL-53(Al)-NH_2 were shown in Figure 1f,g. And the corresponding specific surface area of Fe_3O_4@GO@MIL-53(Al)-NH_2 was 76.75 m^2 g^{-1} and 1.35 nm respectively.

Integrated characterizations involving TEM, FT-IR, XPS, XRD, VSM and BET confirm the successful synthesis of Fe_3O_4@GO@MIL-53(Al)-NH_2.

Table 1. The elemental composition of Fe_3O_4@GO and Fe_3O_4@GO@MIL-53(Al)-NH_2.

Element	Fe_3O_4@GO		Fe_3O_4@GO@MIL-53(Al)-NH_2	
	Atomic Percentage	Mass Percentage	Atomic Percentage	Mass Percentage
Al	0.1	0.1	2.2	3.8
N	0.1	0.1	3.5	3.1
Si	0.1	0.2	1.0	1.7
C	50.0	31.3	59.0	44.8
O	36.8	30.8	29.7	30.0
Fe	12.9	37.5	4.7	16.6

3.2. Optimization of Removal Conditions

To achieve the optimum removal efficiency of perchlorate, several major influencing factors, including the amount of adsorbent, extraction time, and solution pH, were systematically investigated.

3.2.1. Effect of Amount of Adsorbent

An insufficient amount of adsorbent results in low removal efficiency of perchlorate, while an excessive amount of adsorbent raises experimental costs. Accordingly, the amount of adsorbent was evaluated as a critical influencing factor in this work. As illustrated in Figure 2a, the extraction efficiency gradually increased as the amount of adsorbent varied from 10 mg to 200 mg. Nevertheless, no significant improvement in removal efficiency was observed when the amount of adsorbent further increased from 100 mg to 200 mg. Therefore, 100 mg was selected as the optimal amount of adsorbent for subsequent experiments.

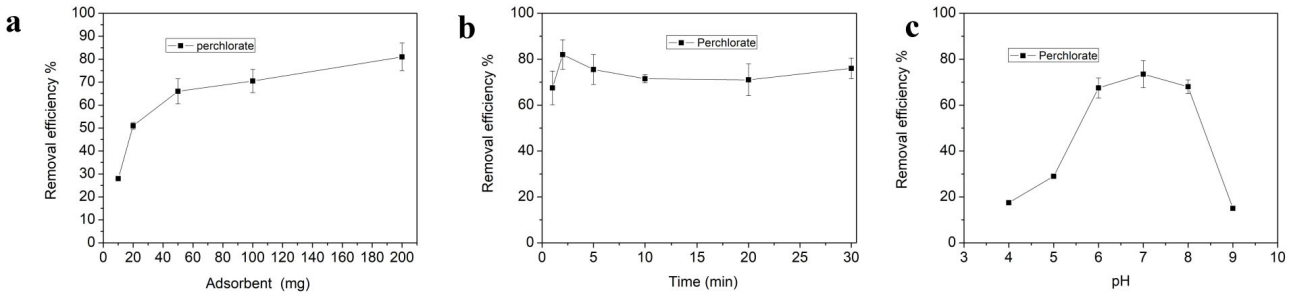


Figure 2. (**a**) Effect of amount of adsorbent on the removal efficiency of perchlorate by Fe_3O_4@GO@MIL-53(Al)-NH_2. Conditions: removal time, 10 min; pH 7; sample volume, 200 mL; analyte concentration: each at 250 μg L^{-1}; n = 3. (**b**) Effect of removal time on the removal efficiency of perchlorate by Fe_3O_4@GO@MIL-53(Al)-NH_2. Conditions: adsorbent amount, 100 mg; pH 7; sample volume, 200 mL; analyte concentration: each at 250 μg L^{-1}; n = 3. (**c**) Effect of solution pH on the removal efficiency of perchlorate by Fe_3O_4@GO@MIL-53(Al)-NH_2. Conditions: adsorbent amount, 100 mg; removal time, 2 min; sample volume, 200 mL; analyte concentration: each at 250 μg L^{-1}; n = 3.

3.2.2. Effect of Removal Time

Removal time is a critical factor affecting the removal efficiency of perchlorate, since insufficient removal time results in low removal efficiency of adsorbents. In this work, stirring-assisted extraction was employed, and the influence of removal time (1–30 min) on the removal of perchlorate was systematically investigated. The corresponding results are presented in Figure 2b. It can be observed that extraction equilibrium was nearly attained when the extraction time exceeded 2 min. Therefore, 2 min was employed as the optimal removal time for the subsequent experiments.

3.2.3. Effect of Solution pH

Perchlorate (ClO_4^-) is a typical inorganic anion; solution pH can alter the surface charge/protonation of the adsorbent in aqueous media and further affect the removal efficiency. The effect of solution pH (4.0–9.0) on perchlorate removal was investigated by adjusting the pH of the sample solution. As shown in Figure 2c, the optimal removal efficiency for perchlorate was obtained at pH 7. Therefore, a solution pH value of 7 was selected for all subsequent experiments in this work.

3.3. Adsorption Kinetics and Isotherms

Adsorption kinetics is an effective approach to explain the mass transfer mechanisms of adsorbates within porous adsorbents. To further explore the transfer mechanisms of perchlorate onto Fe_3O_4@GO@MIL-53(Al)-NH_2, two theoretical kinetic models, namely the pseudo-first-order and the pseudo-second-order, were employed to systematically investigate and quantify the adsorption behavior. Equations (2) and (3) correspond to the pseudo-first-order and pseudo-second-order kinetic models, which are shown as follows.

$$\ln(q_e - q_t) = \ln q_e - k_1 t \quad (2)$$

$$\frac{t}{q_t} = \frac{1}{k_2 q_e^2} + \frac{t}{q_e} \quad (3)$$

$$qe = \frac{(Co - Ce)V}{W} \quad (4)$$

$$qt = \frac{(Co - Ct)V}{W} \quad (5)$$

where t was the adsorption time (min); q_t was the amount of adsorption at time t (mg g^{-1}); q_e was the amount of adsorption at equilibrium time t (mg g^{-1}); K_1 was the pseudo-first-order kinetic constant (min^{-1}); K_2 was the pseudo-second-order kinetic constant (min^{-1});

Plots of the pseudo-first-order and pseudo-second-order models were constructed based on adsorption data obtained at an initial perchlorate concentration of 250 μg L^{-1} and an adsorbent dosage of 20 mg. The q_e and q_t were calculated via Equations (4) and (5). The values of q_e were plotted in Figure 3a, and the corresponding fitting results are summarized in Table 2. A comparison of the kinetic constants calculated via the pseudo-first-order and pseudo-second-order models shows that the correlation coefficient of the pseudo-second-order model (R^2 = 0.9882) was higher than that of the pseudo-first-order model (R^2 = 0.9604). Evidently, the pseudo-second-order model provides a more accurate description of the adsorption process.

In this study, the adsorption capacity of Fe_3O_4@GO@MIL-53(Al)-NH_2 for perchlorate was also investigated. Briefly, 10 mg Fe_3O_4@GO@MIL-53(Al)-NH_2 was added to 1000 mL perchlorate-spiked solutions with initial concentrations ranging from 100 μg L^{-1} to 1000 μg L^{-1} at room temperature, and the results are shown in Figure 3b. The Langmuir and Freundlich isotherm models were applied to fit the equilibrium data, as shown in Equations (6) and (7).

$$\frac{C_e}{Q} = \frac{1}{K_L Q_{max}} + \frac{C_e}{Q_{max}} \quad (6)$$

$$\ln Q = \ln K_F + \frac{1}{n} \ln C_e \quad (7)$$

where C_e was the equilibrium concentration; K_L was the Langmuir constant; Q_{max} was the maximum adsorption capacity (mg/g); K_F was the Freundlich constant; 1/n was a heterogeneity parameter.

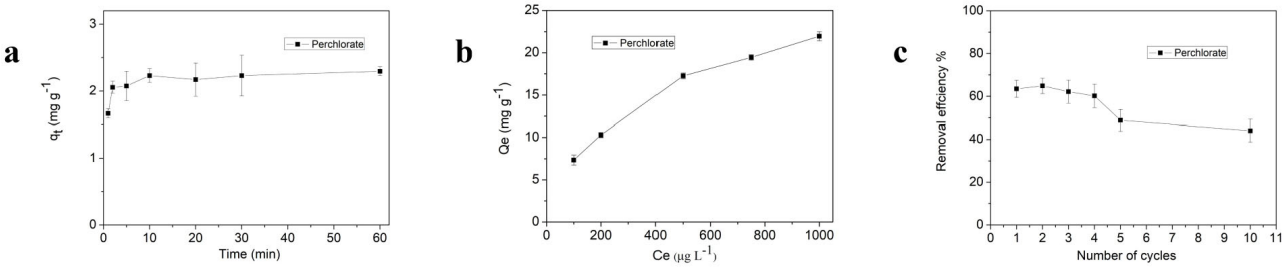


Figure 3. (**a**) Extraction kinetics (qe) of perchlorate by Fe_3O_4@GO@MIL-53(Al)-NH_2. Conditions: adsorbent amount, 20 mg; pH 7; sample volume, 200 mL; analyte concentration: each at 250 μg L^{-1}, *n* = 3. (**b**) Adsorption isotherms of perchlorate by Fe_3O_4@GO@MIL-53(Al)-NH_2. Conditions: adsorbent amount, 20 mg; removal time, 2 min; pH 7; sample volume, 200 mL; analyte concentration: each at 250 μg L^{-1}, *n* = 3. (**c**) Evaluation of the reusability of Fe_3O_4@GO@MIL-53(Al)-NH_2 for perchlorate removal. Conditions: adsorbent amount, 100 mg; removal time, 2 min; pH 7; sample volume, 200 mL; analyte concentration: each at 250 μg L^{-1}.

Table 2. Adsorption kinetic constant and correlation coefficients of pseudo-first-order and pseudo-second-order models.

Kinetic Model	Model Parameters	Perchlorate
pseudo-first-order	k_1/(min^{-1})	1.202
	Q_e (mg g^{-1})	2.29
	R^2	0.9604
pseudo-second-order	k_2/(mg g^{-1} min^{-1})	0.646
	Q_e (mg g^{-1})	2.371
	R^2	0.9882

The adsorption capacity of the Fe_3O_4@GO@MIL-53(Al)-NH_2 toward perchlorate was systematically evaluated. The Langmuir and Freundlich isotherm models were employed to fit the adsorption equilibrium data, and the corresponding fitting parameters are summarized in Table 3. The adsorption of perchlorate by Fe_3O_4@GO@MIL-53(Al)-NH_2 was better described by the Freundlich model (R^2 = 0.9923), compared with the Langmuir model (R^2 = 0.9357). The Qmax of Fe_3O_4@GO@MIL-53(Al)-NH_2 was calculated to be 23.31 mg g^{-1}. The results indicated that the prepared Fe_3O_4@GO@MIL-53(Al)-NH_2 possesses excellent adsorption performance for perchlorate.

Table 3. Adsorption isotherm parameters for perchlorate onto Fe_3O_4@GO@MIL-53(Al)-NH_2.

Model	Model Parameters	Perchlorate
Langmuir	Q_{max} (mg g^{-1})	23.31
	K_L (L μg^{-1})	0.01034
	R^2	0.9357
Freundlich	K_F (mg g^{-1} (μg L^{-1})$^{-1/n}$)	2.38
	1/n	0.334
	R^2	0.9923

3.4. Regeneration and Reusability of Fe_3O_4@GO@MIL-53(Al)-NH_2

Regeneration performance and cycling capacity directly dictate the practical applicability of adsorbent materials. As adsorbents, materials with superior regenerative

reversibility and multi-cycle stability exhibit prominent advantages and can broaden their applicable ranges. In this work, the regeneration performance and reusability of Fe_3O_4@GO@MIL-53(Al)-NH_2 were also systematically investigated. The regeneration procedure for Fe_3O_4@GO@MIL-53(Al)-NH_2 was performed in accordance with the description in Section 2.5. After each regeneration cycle, Fe_3O_4@GO@MIL-53(Al)-NH_2 was reused to assess its recyclability, and the corresponding results are presented in Figure 3c. As illustrated in Figure 3c, the removal efficiency of perchlorate exhibited no obvious decline within the first four cycles. However, a gradual reduction in removal efficiency was observed from the 5th to the 10th cycle, demonstrating that Fe_3O_4@GO@MIL-53(Al)-NH_2 can sustain stable adsorption performance for at least four cycles.

3.5. Removal Mechanism

In this work, the removal mechanism of Fe_3O_4@GO@MIL-53(Al)-NH_2 for removing perchlorate was investigated. The perchlorate removal efficiencies of Fe_3O_4, Fe_3O_4@GO, Fe_3O_4@MIL-53(Al)-NH_2 and Fe_3O_4@GO@MIL-53(Al)-NH_2 was compared. As shown in Figure 4a, Fe_3O_4@GO@MIL-53(Al)-NH_2 exhibited a significantly higher perchlorate removal efficiency than Fe_3O_4, Fe_3O_4@GO and Fe_3O_4@MIL-53(Al)-NH_2. As a single-layer carbonaceous adsorbent, GO possesses abundant functional groups on its surface, such as hydroxyl, carboxyl, and epoxy groups. The adsorption of perchlorate by GO is primarily driven by hydrophobic interactions and intermolecular hydrogen bonding. The introduction of MOFs (MIL-53(Al)-NH_2) further improves the removal efficiency via the size exclusion effect. Accordingly, it can be inferred that the perchlorate adsorption by Fe_3O_4@GO@MIL-53(Al)-NH_2 may rely on the combined effects of hydrophobic interaction, intermolecular hydrogen bonding, and the size exclusion effect.

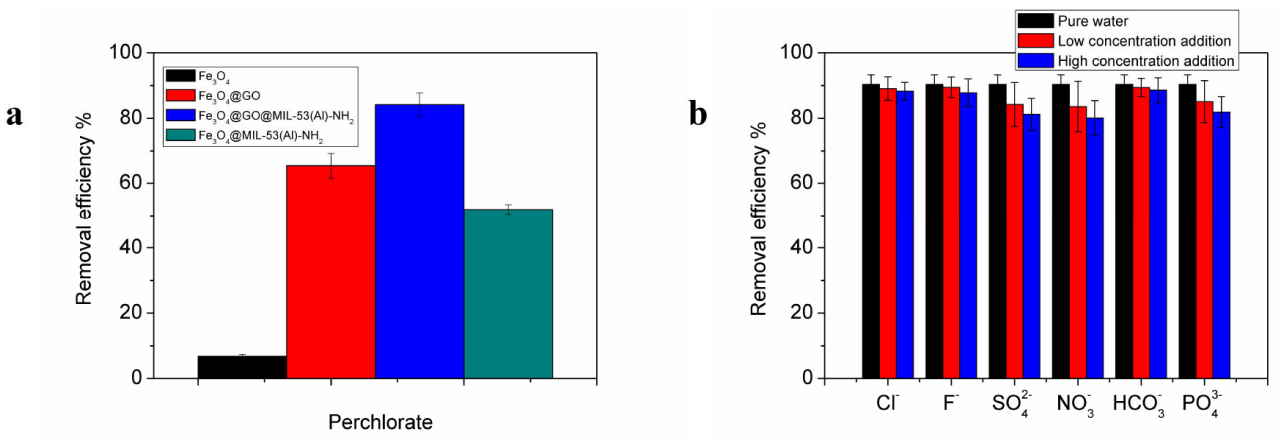


Figure 4. (**a**) Comparison of the removal efficiency of perchlorate by Fe_3O_4, Fe_3O_4@GO, Fe_3O_4@MIL-53(Al)-NH_2 and Fe_3O_4@GO@MIL-53(Al)-NH_2. Conditions: adsorbent amount, 100 mg; removal time, 2 min; pH 7; sample volume, 200 mL; analyte concentration: each at 250 μg L^{-1}, n = 3. (**b**) The effect of co-existing anion on the removal efficiency of perchlorate, the low concentration addition of each anion (Cl^-, NO_3^-, SO_4^{2-}, HCO^{3-}, PO_4^{3-} and F^-) was 0.5 mg L^{-1}, 10 mg L^{-1}, 10 mg L^{-1}, 10 mg L^{-1}, 10 mg L^{-1} and 10 mg L^{-1}, respectively; the high concentration addition of each anion (Cl^-, NO_3^-, SO_4^{2-}, HCO^{3-}, PO_4^{3-} and F^-) was 2.5 mg L^{-1}, 50 mg L^{-1}, 50 mg L^{-1}, 50 mg L^{-1}, 50 mg L^{-1} and 50 mg L^{-1}, respectively. Conditions: adsorbent amount, 100 mg; removal time, 2 min; pH 7; sample volume, 200 mL; analyte concentration: each at 250 μg L^{-1}; n = 3.

3.6. Co-Existing Anions Interference

Various inorganic anions, including Cl^-, NO_3^-, SO_4^{2-}, HCO_3^-, PO_4^{3-} and F^-, ubiquitously exist in natural water samples, which can compete with ClO_4^- for available adsorption sites and thereby interfere with the removal efficiency. Hence, it is essential

to investigate the influences of co-existing anions on the adsorption of perchlorate over Fe_3O_4@GO@MIL-53(Al)-NH_2. Considering the actual concentration ranges of anions in environmental water, a series of concentration gradients for coexisting anions was chosen to evaluate the interference on perchlorate removal performance. The perchlorate removal performance was investigated in pure water solution and solutions containing different interfering anions, and the corresponding results are shown in Figure 4b. It can be concluded from the obtained data that Cl^-, F^-, $SO_4{}^{2-}$, $HCO_3{}^-$, $PO4^{3-}$ and $NO_3{}^-$ barely affect $ClO_4{}^-$. Overall, co-existing diverse interfering ions in environmental water exert no significant adverse impact on the perchlorate removal performance of Fe_3O_4@GO@MIL-53(Al)-NH_2.

3.7. Removal Efficiency of Perchlorate and Comparison with Other Methods

Under optimum conditions (adsorbent amount, 100 mg; removal time, 2 min; pH 7; sample volume, 200 mL; water: deionized water; n = 3), Fe_3O_4@GO@MIL-53(Al)-NH_2 was applied for the removal of perchlorate and its removal efficiency was systematically evaluated. A favorable removal efficiency of 90.2 ± 5.1% (spiked concentration was 250 μg L^{-1}) was obtained in this work.

A comparison of Qmax obtained by this method with other similar methods is summarized in Table 4. The Qmax of Fe_3O_4@GO@MIL-53(Al)-NH_2 was higher than the methods of granular ferric hydroxide [34], carbon nanotubes [35], single-walled carbon nanotubes [36], magnetized and quaternary amine-functionalized bio-resin derived from corn stalk [37]; lower than the methods of cationic MOFs (ESC) [38], Mg/Fe hydrotalcite [39], $FeCl_3$/DDAC-modified activated [40] and Zr(IV)-CTS [41].

Table 4. Comparison of sorbent dosage, removal time, volume, concentration, and Qmax with other methods for removal of perchlorate.

Adsorption Materials	Sorbent Dosage	Removal Time	Volume	Concentration	Q_{max}	References
Granular ferric hydroxide	1.0 g L^{-1}	24 h	-	500 mg L^{-1}	20 mg g^{-1}	[34]
CNTs	solid-solution rate,10:1	24 h	8 mL	-	3.55 mg g^{-1}	[35]
SWCNTs	0.5 g L^{-1}	8 h	1 L	-	6 mg g^{-1}	[36]
Cationic MOFs (ESC)	0.2 g	24 h	100 mL	-	143.48 mg g^{-1}	[38]
Mg/Fe hydrotalcite	0.1 g	24 h	100 mL	-	91.33 mg g^{-1}	[39]
CS-MNB	0.1 g	24 h	-	100 mg L^{-1}	23.16 mg g^{-1}	[37]
$FeCl_3$/DDAC-modified activated carbon	0.2 g	4 h	200 mL	50 mg L^{-1}	31.69 mg g^{-1}	[40]
Zr(IV)-CTS	0.05 g	1.5 h	100 mL	500 mg L^{-1}	133.69 mg g^{-1}	[41]
Fe_3O_4@GO@MIL-53(Al)-NH_2	0.02 g	2 min	200 mL	250 mg L^{-1}	23.31 mg g^{-1}	This work

Fe-CB, Fe (III)–chitosan complex. CNTs, carbon nanotubes. SWCNTs, single-walled carbon nanotubes. ESC, ethanedisulfonic. CS-MNB, magnetized and quaternary amine-functionalized bio-resin derived from corn stalk. DDAC, quaternary ammonium salt dodecyldimethylammonium chloride. CTS, chitosan.

A notable advantage of the proposed method over those methods was its rapid extraction kinetics (2 min vs. 1.5–24 h).

3.8. Removal Effect in Real Environmental Water Samples

The proposed method was used to remove perchlorate in real environmental water samples. The real environmental water sample was collected from the Xiangjiang River

(Changsha, China). The pH value of the river water was 7.2. The natural water matrix contains various inorganic ions, including Cl^-, NO_3^-, SO_4^{2-}, F^-, ClO_4^-, and their concentrations were 67 μg L^{-1}, 1.01 mg L^{-1}, 4.56 mg L^{-1}, 80 μg L^{-1}, 1.01 mg L^{-1}, and 15 μg L^{-1}, respectively. Then a good removal performance with a removal efficiency of 82.2 ± 4.3% was obtained in this work. The corresponding chromatograms of perchlorate-spiked water samples before and after removal are shown in Figure 5. The results demonstrate that the proposed method achieves favorable removal efficiency for real drinking water samples and can satisfy the requirements for perchlorate removal in drinking water in China.

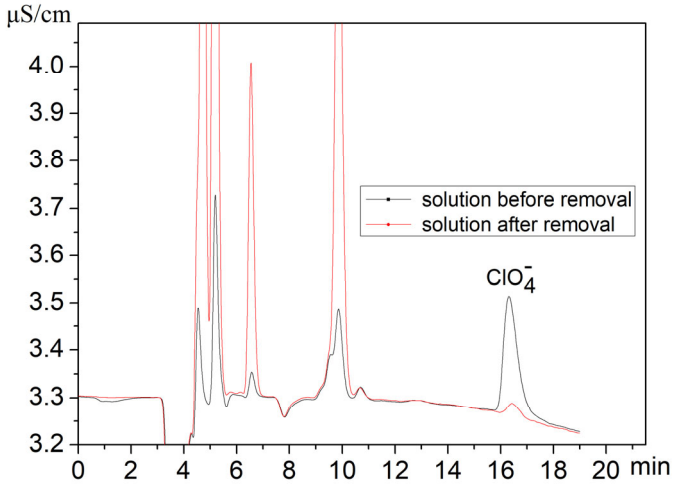


Figure 5. The ion chromatograms of perchlorate-spiked water samples before and after adsorption removal. Conditions: adsorbent amount, 100 mg; removal time, 2 min; pH 7; sample volume, 200 mL; spiked concentration: 250 μg L^{-1}.

4. Conclusions

In this work, a novel magnetic nanocomposite (Fe_3O_4@GO@MIL-53(Al)-NH_2) was successfully prepared and systematically characterized. Integrating the advantageous properties of GO and MOFs, Fe_3O_4@GO@MIL-53(Al)-NH_2 exhibits fast extraction kinetics, large specific surface area, and high extraction efficiency. Furthermore, Fe_3O_4@GO@MIL-53(Al)-NH_2 was employed for the removal of perchlorate from real environmental water samples. Benefiting from simple operation, rapid extraction kinetics, and remarkable removal efficiency, the proposed method demonstrates great application potential for perchlorate removal in diverse aqueous environments.

Author Contributions: Methodology, Z.B.; Investigation, M.X.; Data curation, L.Y.; Writing—original draft, C.H.; Writing—review and editing, Q.W.; Visualization, Y.D. All authors have read and agreed to the published version of the manuscript.

Funding: This project was funded by the Hunan Provincial Natural Science Foundation of China (No. 2025JJ80517), Changsha Municipal Natural Science Foundation (No. Kq2208483), Scientific research project of the Hunan Provincial Health Commission (Nos. D202312066318 and 20256116), and support by the project of Hunan Province health high-level talents.

Institutional Review Board Statement: Not applicable.

Informed Consent Statement: Not applicable.

Data Availability Statement: The original contributions presented in this study are included in the article. Further inquiries can be directed to the corresponding authors.

Conflicts of Interest: The authors have declared no conflicts of interest.

References

1. Cao, F.; Jaunat, J.; Sturchio, N.; Cancès, B.; Morvan, X.; Devos, A.; Barbin, V.; Ollivier, P. Worldwide occurrence and origin of perchlorate ion in waters: A review. *Sci. Total Environ.* **2019**, *661*, 737–749. [CrossRef]
2. Hu, J.; Xian, Y.; Wu, Y.; Chen, R.; Dong, H.; Hou, X.; Liang, M.; Wang, B.; Wang, L. Perchlorate occurrence in foodstuffs and water: Analytical methods and techniques for removal from water—A review. *Food Chem.* **2021**, *360*, 130146. [CrossRef]
3. Mathew, J.; Gandhi, J.; Hedrick, J. Trace level perchlorate analysis by ion chromatography-mass spectrometry. *J. Chromatogr. A* **2005**, *1085*, 54–59. [CrossRef]
4. Fang, C.; Naidu, R. A review of perchlorate contamination: Analysis and remediation strategies. *Chemosphere* **2023**, *338*, 139562. [CrossRef]
5. Hu, Z.; Jia, Y.; Wu, Y.; Zhang, Y. Occurrence and removal technologies of perchlorate in water: A systematic review and bibliometric analysis. *Chemosphere* **2024**, *364*, 143119. [CrossRef]
6. Dong, H.; Xiao, K.; Xian, Y.; Wu, Y.; Zhu, L. A novel approach for simultaneous analysis of perchlorate (ClO_4^-) and bromate (BrO_3^-) in fruits and vegetables using modified QuEChERS combined with ultrahigh performance liquid chromatography-tandem mass spectrometry. *Food Chem.* **2019**, *270*, 196–203. [CrossRef]
7. Tang, Y.; Zhong, B.; Qu, B.; Feng, S.; Ding, S.; Su, S.; Li, Z.; Gan, Z. Occurrence of perchlorate in groundwater, paired farmland soil, lettuce, and rhizosphere soil from Chengdu, China. *Environ. Sci. Process. Impacts* **2017**, *19*, 752–757. [CrossRef]
8. Krishnan, G.R.; Prabhakaran, K.; George, B.K. N-doped activated carbon with hierarchical pores for the efficient removal of perchlorate from water. *Microporous Mesoporous Mater.* **2021**, *315*, 110892. [CrossRef]
9. *GB/T 5750-2023*; Standard Examination Methods for Drinking Water. Standards Press of China: Beijing, China, 2023.
10. Ford, C.L.; Park, Y.J.; Matson, E.M.; Gordon, Z.; Fout, A.R. A bioinspired iron catalyst for nitrate and perchlorate reduction. *Science* **2016**, *354*, 741–743. [CrossRef]
11. Aarthi, T.; Madras, G. Photocatalytic degradation of rhodamine dyes with nano-TiO_2. *Ind. Eng. Chem. Res.* **2007**, *46*, 7–14. [CrossRef]
12. Wan, D.; Li, Q.; Chen, J.; Niu, Z.; Liu, Y.; Li, H.; Xiao, S. Simultaneous bio-electrochemical reduction of perchlorate and electro-disinfection in a novel Moving-Bed Biofilm Reactor (MBBR) based on proton-exchange membrane electrolysis. *Sci. Total Environ.* **2019**, *679*, 288–297. [CrossRef]
13. Ao, J.; Wang, Y.; Bu, L.; Wu, Y.; Xiao, J.; Zhou, S.; Wang, S. Imine-Linked Covalent Organic Frameworks Tuned by Quaternary-Ammonium-Alkyl for Highly Effective and Selective Adsorption of Perchlorate from Water. *Small* **2025**, *21*, e2501400. [CrossRef]
14. Hou, P.; Yan, Z.; Cannon, F.S.; Yue, Y.; Byrne, T.; Nieto-Delgado, C. Enhancement of perchlorate removal from groundwater by cationic granular activated carbon: Effect of preparation protocol and surface properties. *Chemosphere* **2018**, *201*, 756–763. [CrossRef]
15. Jin, S.; Liu, L.; Li, S.; Zhou, Y.; Huang, C.; Wang, Z.; Zhai, Y. Removal of low concentration of perchlorate from natural water by quaternized chitosan sphere (CGQS): Efficiency and mechanism research. *J. Hazard. Mater.* **2024**, *466*, 133595. [CrossRef]
16. Ren, Z.; Xu, X.; Gao, B.; Li, Y.; Kong, J.; Shang, Y.; Song, W.; Zhang, Q. Capture of perchlorate by a surface-modified bio-sorbent and its bio-regeneration properties: Adsorption, computations and biofouling. *Chemosphere* **2017**, *185*, 152–161. [CrossRef]
17. Xu, J.; Gao, N.; Zhao, D.; An, N.; Li, L.; Xiao, J. Bromate reduction and reaction-enhanced perchlorate adsorption by $FeCl_3$-impregnated granular activated carbon. *Water Res.* **2019**, *149*, 149–158. [CrossRef]
18. Xu, J.H.; Gao, N.Y.; Deng, Y.; Sui, M.H.; Tang, Y.L. Perchlorate removal by granular activated carbon coated with cetyltrimethyl ammonium bromide. *J. Colloid Interface Sci.* **2011**, *357*, 474–479. [CrossRef]
19. Lehman, S.G.; Badruzzaman, M.; Adham, S.; Roberts, D.J.; Clifford, D.A. Perchlorate and nitrate treatment by ion exchange integrated with biological brine treatment. *Water Res.* **2008**, *42*, 969–976. [CrossRef]
20. Song, W.; Gao, B.; Wang, H.; Xu, X.; Xue, M.; Zha, M.; Gong, B. The rapid adsorption-microbial reduction of perchlorate from aqueous solution by novel amine-crosslinked magnetic biopolymer resin. *Bioresour. Technol.* **2017**, *240*, 68–76. [CrossRef]
21. Li, T.; Ren, Y.; Zhai, S.; Zhang, W.; Zhang, W.; Hua, M.; Lv, L.; Pan, B. Integrating cationic metal-organic frameworks with ultrafiltration membrane for selective removal of perchlorate from Water. *J. Hazard. Mater.* **2020**, *381*, 120961. [CrossRef]
22. Wang, P.L.; Xie, L.H.; Joseph, E.A.; Li, J.R.; Su, X.O.; Zhou, H.C. Metal-Organic Frameworks for Food Safety. *Chem. Rev.* **2019**, *119*, 10638–10690. [CrossRef]
23. Yuan, S.; Feng, L.; Wang, K.; Pang, J.; Bosch, M.; Lollar, C.; Sun, Y.; Qin, J.; Yang, X.; Zhang, P.; et al. Stable Metal-Organic Frameworks: Design, Synthesis, and Applications. *Adv. Mater.* **2018**, *30*, e1704303. [CrossRef]
24. Li, D.; He, M.; Chen, B.B.; Hu, B. Metal organic frameworks-derived magnetic nanoporous carbon for preconcentration of organophosphorus pesticides from fruit samples followed by gas chromatography-flame photometric detection. *J. Chromatogr. A* **2019**, *1583*, 19–27. [CrossRef]
25. Mohan, B.; Kamboj, A.; Virender; Singh, K.; Priyanka; Singh, G.; Pombeiro, A.J.L.; Ren, P. Metal-organic frameworks (MOFs) materials for pesticides, heavy metals, and drugs removal: Environmental safety. *Sep. Purif. Technol.* **2023**, *310*, 20. [CrossRef]

26. Nabil, M.; Abdel-Gawad, H.; Elantabli, F.M.; El-Medani, S.M.; Abdelhameed, R.M. Removal Method of Pesticides and Their Improvement Using Metal-Organic Frameworks. *Egypt. J. Chem.* **2023**, *66*, 39–75. [CrossRef]
27. Li, R.X.; Zhong, W.B.; Xie, L.H.; Xie, Y.B.; Li, J.R. Recent Advances in Adsorption removal of Cr ions by metal-organic frameworks. *Chin. J. Inorg. Chem.* **2021**, *37*, 385–400. [CrossRef]
28. Moslem, A.; Negin, N.; Farzaneh, E.N.; Mehdi, K.; Saeid, A.; Maryam, D.; Roya, J. Phytochemical-mediated design of magnetic $MgFe_2S_4$/$CoBiO_2I$ heterojunction for enhanced photocatalytic degradation of Ciprofloxacin. *J. Saudi. Chem. Soc.* **2026**, *30*, 68. [CrossRef]
29. Farzaneh, E.N.; Mohammad, A.N.; Morteza, G.; Negin, N. Highly efficient solar-driven photocatalytic degradation of ciprofloxacin from aqueous solution using a novel metal–organic framework catalyst. *Appl. Water. Sci.* **2026**, *16*, 93. [CrossRef]
30. Ahmadi, M.; Elmongy, H.; Madrakian, T.; Abdel-Rehim, M. Nanomaterials as sorbents for sample preparation in bioanalysis: A review. *Anal. Chim. Acta* **2017**, *958*, 1–21. [CrossRef]
31. Ibrahim, W.A.; Nodeh, H.R.; Sanagi, M.M. Graphene-Based Materials as Solid Phase Extraction Sorbent for Trace Metal Ions, Organic Compounds, and Biological Sample Preparation. *Crit. Rev. Anal. Chem.* **2016**, *46*, 267–283. [CrossRef]
32. Taghvimi, A.; Hamishehkar, H.; Ebrahimi, M. Magnetic nano graphene oxide as solid phase extraction adsorbent coupled with liquid chromatography to determine pseudoephedrine in urine samples. *J. Chromatogr. B* **2016**, *1009*, 66–72. [CrossRef]
33. Xue, B.; Xu, M.Z.; Bai, Z.H.; Hu, C. The determination of estrogens in fish samples by magnetic solid phase extraction couple to high performance liquid chromatography—Diode array detector. *Adv. Sample Prep.* **2024**, *11*, 100120. [CrossRef]
34. Kumar, E.; Bhatnagar, A.; Choi, J.A.; Kumar, U.; Min, B.; Kim, Y.; Song, H.; Paeng, K.J.; Jung, Y.M.; Abou-Shanab, R.A.I.; et al. Perchlorate removal from aqueous solutions by granular ferric hydroxide (GFH). *Chem. Eng. J.* **2010**, *159*, 84–90. [CrossRef]
35. Fang, Q.; Chen, B. Adsorption of perchlorate onto raw and oxidized carbon nanotubes in aqueous solution. *Carbon* **2012**, *50*, 2209–2219. [CrossRef]
36. Hsu, Y.S.; Lou, J.C.; Chou, M.S.; Hsu, K.L.; Han, J.Y. Characterization of single walled carbon nanotubes and adsorption of perchlorate in water. *Water Air Soil Pollut.* **2015**, *226*, 58. [CrossRef]
37. Pan, J.; Gao, B.; Song, W.; Xu, X.; Jin, B.; Yue, Q. Column adsorption and regeneration study of magnetic biopolymer resin for perchlorate removal in presence of nitrate and phosphate. *J. Clean. Prod.* **2019**, *213*, 762–775. [CrossRef]
38. Zhang, H.; Li, T.; Yang, Z.; Su, M.; Hou, L.; Chen, D.; Luo, D. Highly efficient removal of perchlorate and phosphate by tailored cationic metal-organic frame works based on sulfonic ligand linking with Cu-4,4′-bipyridyl chains. *Sep. Purif. Technol.* **2017**, *188*, 293–302. [CrossRef]
39. Liu, Y.; Liu, Y.; He, Q.; Guo, P.; Chen, J.; Wan, D.; Xiao, S. Utilizing the "memory effect" of bimetallic-supported hydrotalcites for adsorption and reduction of perchlorate in water. *Colloids Surf. A* **2020**, *593*, 124641. [CrossRef]
40. Hu, Z.H.; Wu, Y.; Wei, J.G.; Yan, J.; Dai, X.N.; Huang, J.L.; Zhang, Y. Valency-regulated interfacial selectivity by metal-crosslinked chitosan cryogels for capturing trace-level perchlorate: Adsorption performance and mechanism. *Carbohydr. Polym.* **2026**, *390*, 125736. [CrossRef]
41. Shan, Y.X.; Jia, Y.N.; Wu, X.M.; Xu, N.N.; Liu, Z.D.; Li, L.; Wang, Z.W.; Feng, W.T.; Gong, W.X.; Cui, H.C.; et al. Adsorption of perchlorate in water by $FeCl_3$/dodecyldimethylammonium-chloride-modified activated carbon: Synergistic effect and mechanistic study. *Small* **2025**, *21*, 8. [CrossRef]

Disclaimer/Publisher's Note: The statements, opinions and data contained in all publications are solely those of the individual author(s) and contributor(s) and not of MDPI and/or the editor(s). MDPI and/or the editor(s) disclaim responsibility for any injury to people or property resulting from any ideas, methods, instructions or products referred to in the content.